Organ-Dedicated Molecular Imaging Systems

Antonio J. González, Filomeno Sánchez, and José M. Benlloch

***Abstract*— In this review we will cover both clinical and technical aspects of the advantages and disadvantages of organ specific (dedicated) molecular imaging systems, namely PET and SPECT, including gamma cameras. This review will start with the introduction to the organ-dedicated molecular imaging systems. Thereafter we will describe the differences and their advantages/disadvantages when compared with the standard large size scanners. We will review time evolution of dedicated systems, from first attempts to current scanners, and the ones that ended in clinical use. We will review later the state of the art of these systems for different organs, namely: breast, brain, heart, and prostate. We will also present the advantages offered by these systems as a function of the special application or field, such as in surgery, therapy assistance and assessment, etc. Their technological evolution will be introduced for each organ-based imager.**

Some of the advantages of dedicated devices are: higher sensitivity by placing the detectors closer to the organ, improved spatial resolution, better image contrast recovery (by reducing the noise from other organs), and also lower cost. Designing a complete ring-shaped dedicated PET scanner is sometimes difficult and limited angle tomography systems are preferable as they have more flexibility in placing the detectors around the body/organ. Examples of these geometries will be presented for breast, prostate and heart imaging. Recently achievable excellent TOF capabilities below 300 ps FWHM reduce significantly the impact of missing angles on the reconstructed images.

Index Terms—Organ dedicated PET, organ specific/dedicated SPECT, Nuclear Medicine, compact equipment.

I. Introduction

MOLECULAR Imaging includes several imaging techniques. The main are Positron Emission Tomography (PET) [1], Gamma Cameras and Single Photon Emission Computed Tomography (SPECT) [2]. These imaging modalities are also known as functional imaging since they provide information on the biological processes occurring in the patient body. Fluorescence imaging can be considered as an alternative molecular imaging technique but its low penetration range (few millimeters) reduces its application field. Other imaging techniques provide anatomical or morphological information about the different patient's organs and tissues. The most important anatomical imaging techniques are Magnetic Resonance Imaging (MRI), Computed Tomography (CT) and Ultrasounds (US). Functional magnetic resonance imaging or functional MRI (fMRI) measures brain activity by detecting changes associated with blood flow. This technique relies on the fact that cerebral blood flow and neuronal activation are coupled. Those non Molecular Imaging techniques primarily visualize the structure of the organ and, sometimes, its dynamics. These data do not provide direct functional metabolic information on the tissue status. In contrast, Molecular Imaging provides functional organ information. Hybrid imaging systems, typically combining molecular and morphologic information have been developed and have currently widespread use in nuclear medicine departments (PET/CT, SPECT/CT). More recently PET/MR has been proposed showing promising preclinical and clinical cardiac applications where it could play a substantial role [3]. Specific, organ-dedicated, nuclear medicine imaging devices could allow one to carry out accurate new studies due to a high sensitivity, high spatial resolution and high signal-to-noise ratio.

When dealing with Molecular Imaging (MI) studies involving systemic injection of radiolabelled imaging agents into the patient, the issue of radiation exposure became recently one of the critical aspects associated to nuclear medicine. This requires a new radical approach in the future developments of Molecular Imaging systems to increase sensitivity as much as possible. For that reason, dedicated specific systems with modular and optimized geometry, in order to attain the highest possible angular coverage of the dedicated organ, are desirable.

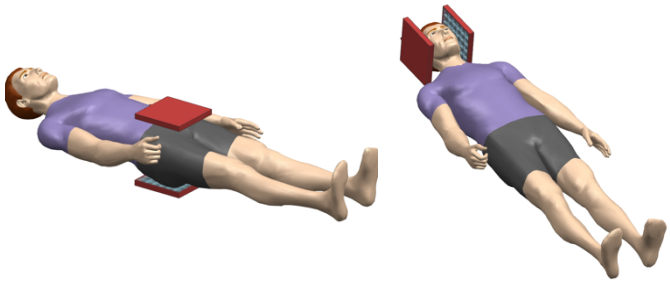

(a) (b)

Fig. 1. Representation of applications using two panels PET, prostate and brain imagers, (a) and (b) sketches, respectively.

In this review we will concentrate on the aforementioned PET, SPECT and some Gamma Camera techniques, with focus on organ specific designs, also known as dedicated systems. See for instance in Fig. 1 sketches for two-panel detector approach applied to brain and prostate PET systems. One of the aims of this work is to show the reader the advantages and disadvantages of organ-dedicated MI systems,

Manuscript submitted on 17th March 2018.

F. Sanchez, J.M. Benlloch and A.J. González are with the Instituto de Instrumentación para Imagen Molecular (I3M), Centro Mixto CSIC — Universitat Politècnica de València, Camino de Vera s/n, 46022 Valencia, SPAIN (e-mail: agonzalez@i3m.upv.es).

especially when compared to large size (whole body) scanners. We will describe the technological evolution and developments carried out on dedicated clinical systems. We will review both the currently existing research and commercially available MI devices, as well as future trends. The authors would like to point out that in this work it has been tried to cite most of the known developments or design trends, but most likely some have been, unfortunately and non-intentionally, omitted.

This review is organized with first a brief description and basic principles of the most known molecular imaging systems, including some history evolution and main instrumental components. This is followed by a description of these systems applied to different organs, starting from brain, to breast and then later to heart. In these sections there are descriptions of some of the systems that most have been shown in the literature, differentiating them from standard gamma cameras, PET, or SPECT systems. There are also descriptions of the combinations of these systems with other modalities (MR or CT). Later, this review describes other organ-dedicated ideas and projects that could benefit early the patient, and improve the diagnostic and treatment assessment quality available to clinicians.

II. MI Systems

A. Gamma camera

A Gamma Camera (GC) system employs the lowest number of components associated with an MI scanner. Typical designs for a GC include a physical heavy metal collimator, a scintillation crystal and a photosensor. Other designs are based on solid state technology such as Cadmium Zinc Telluride (CZT). The earlier GC systems were based on scintillation materials but nowadays CZT designs are becoming more efficient and also more successfully used.

In the simpler GC as well as in the tomographic SPECT technique, the patient is injected with a single gamma ray emitting tracer. The administration method depends on the organ and pathology to be examined. Although intravenous or intratumoral injections are the most used, in breast cancer also peritumoral is used. Gamma rays are emitted from the high activity regions in the patient's body where the imaging agent is present, and finding their sources of emission is the key objective of MI systems. One of the most used radioisotopes in GC is ^{99m}Tc, emitting a gamma ray with an energy of 140 keV. There are specific isotopes with energies of emitted gamma rays ranging from 30 to 350 keV. GC designs are not typically designed covering the whole energy range, since they are optimized for the particular application and the radioisotope used.

Several collimator types are used depending mainly on the application, in order to provide position information of the points of emission of the gamma rays. Although sensitivity and spatial resolution for pinhole collimators significantly deteriorates as the source to collimator distance increases, this also increases the GC Field of View (FOV). In this sense, for applications to small organs, pinhole collimators could be desirable in order to increase the FOV at the object plane. The hole diameter of the pinhole collimator must be selected as a trade off between the spatial resolution, expected distance to the imaged object, and the sensitivity of the system. Parallel hole collimators, when dealing with organ-dedicated GC do not allow to increase the FOV, and although its sensitivity does not depend on the source-detector distance and its spatial resolution is equivalent to that obtained with pinhole collimators, they are more widely used in standard general purpose GCs.

Another widely used type is the multi-pinhole collimator based on many pinholes. This last approach is a compromise between spatial resolution and sensitivity. Gamma rays going through the collimator are stopped in the scintillation or solid state material. In the case of the scintillation material, a number of visible photons are generated depending on the stopped gamma ray energy. Scintillation crystals used in GC are NaI, CsI (Na or Tl doped) but also other with higher effective atomic numbers such as BGO or GAGG. Gamma cameras operate in the so-called single gamma mode and, therefore, all these crystals should not contain natural radioactivity. The scintillation light is transferred to the photosensor element and converted into a measurable signal pulse. In the case of CZT detectors, the conversion is directly done at the "crystal". Several photosensor types and arrangements have been used and will be described in the coming sections. Electronics associated with the treatment of the signal pulses make it possible to return an accurate impact position within the crystal and, therefore, deduce the point of emission.

First clinical gamma camera designs were possible after the development of the Anger scintillation camera concept in 1957 [4]. Its large detector face was able to capture emitted simultaneously gamma emissions from larger areas of the body, thus increasing the detection efficiency of gamma photons, as compared to the non-imaging gamma probes.

B. Single Photon Emission Computed Tomography

SPECT systems are mainly based on multiple GCs mounted to a rotation stage and allowing retrieving the tomographic 3D information about the imaging agent's distribution in the body, after image reconstruction. Typically, the angular step between consecutive single image projections varies from 3 to 6 degrees, covering all 360 degrees. Similarly to GC, several types of collimators, scintillators and photosensors, as well as CZT technology are found in SPECT systems.

In contrast to GC, SPECT provides much more than planar projective information as it allows for accurate functional 3D information, after the reconstruction process performed by dedicated software algorithms. There is a broad variety of available radiotracers, making possible a high number of SPECT applications such as brain functional studies, heart, bone analysis or lung, to name a few. Best known SPECT

applications in brain imaging are blood perfusion to study dementia, epilepsy or TBI (Traumatic Brain Injury). Another widely used application of SPECT in brain studies is the use of ligand neuroreceptors as imaging agents. SPECT technology is used in heart imaging as well, studying the myocardium tissue functionality, for example in order to discriminate between ischemia and infarct.

C. Positron Emission Tomography

The basic detector technology of PET scanners is similar to GC. However, no physical collimator is used due to the PET coincidence principle with the simultaneous detection of two annihilation photons. In PET, patients are injected with a positron emitter radiotracer. One of the major factors contributing to the acceptance of PET was the development of ^{18}F labeled 2-fluorodeoxy-glucose (2FDG). In particular, ^{18}F emits positrons with an energy nearing 600 keV. Positrons annihilates with electrons in the tissue or medium producing two approximately back-to-back photons with characteristic 511 keV energy. Although higher energies than in GC (or SPECT) are present in PET, one of the advantages of the design is that it needs to be only optimized for a particular one energy of 511 keV. In the PET principle, two opposed GC type detectors (without physical collimator) measure in coincidence the two emitted gamma photons. The line connecting the two detected 511 keV conversion points in the two detectors is known as Line of Response (LOR). After a complex image reconstruction process, as in the case of SPECT, a tomographic emission image is generated. The sensitivity in PET is significantly higher by many orders of magnitude than in the case of SPECT given the lack of the physical collimation.

PET scanners (also SPECT and GC) must be very sensitive in order to fulfill the tracer principle: the molecules that are injected in the body should not modify the regular behavior of the biosystem. In fact, PET has at least a million fold sensitivity advantage over other imaging modalities, for instance when imaging studies of metabolism and neuroreceptor activity.

In 1973, Robertson and collaborators built the first PET ring scanner but were unable to obtain true reconstructed cross sectional images. Phelps and Ter-Pogossian [5][6] published the principles of modern PET and their design led to the production of the first commercial PET scanner. PET has become the technique of choice for static and dynamic imaging of biological biomarkers in human patients and in animals.

III. Brain Imaging Systems

A. Brain PET

It is interesting to notice that the first PET scanner was already a dedicated brain PET system, proposed by Brownell and Aronow in 1952. Brain PET instrumentation has greatly evolved from its infancy, when it was used in regional localization, to currently providing excellent resolution with imaging characteristics that can greatly impact clinical management [7]. In this subsection, a review of stand-alone PET systems will be carried out first, followed by brain imaging implementations using SPECT technology. Last sub-section is dedicated to brain systems that can sequentially or simultaneously be combined with complementary information (CT or MRI).

It was in the 90's when the High Resolution Research Tomograph (HRRT) was launched [8][9], a brain dedicated PET. Two prototypes were initially constructed, see example photograph in Fig. 2 (a). A double layer prototype consisted of five detector heads with two 7.5 mm thick LSO layers and three detector heads with an LSO layer and a GSO layer, both 7.5 mm thick. A single layer prototype had only one layer of LSO crystals. The commercial version consisted of eight detector heads. Each detector head contains 117 detector blocks arranged in a 9 × 13 array which are read out by a 10 × 14 array of photomultiplier tubes (PMTs). Each detector block (19 mm × 19 mm × 20 mm) is cut into 8 × 8 crystal elements. The system defines a FOV of 312 mm in diameter and 250 mm in axial length. A spatial resolution in the range of 2.3 - 3.2 mm (FWHM) in the transaxial direction and 2.5 - 3.4 mm in the axial direction have been reported. Absolute line-source sensitivity ranged from 2.5 to 3.3%. Maximum NECR was 45 kcps and 148 kcps according to the NEMA-2001 and 1994 protocols, respectively.

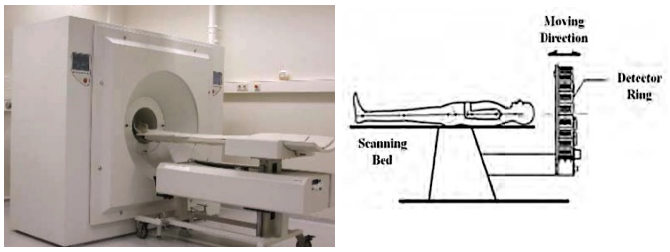

(a) (b)

Fig. 2. (a) Photograph of the HRRT from [8] © Institute of Physics and Engineering in Medicine. Reproduced by permission of IOP Publishing. All rights reserved. (b) Sketch of the Rainbow VHD PET [10].

The concept of supine position has been followed by the Rainbow VHD PET [10], as shown in Fig. 2 (b). One of the particularities of its detector block design is the inclusion of a small PMT in the centre between 4 larger PMTs in order to better identify the LYSO crystal elements in the gap between the large PMTs. The PET ring has a diameter of 463 mm aperture and, defines a transaxial and axial FOVs of 256 mm and 120 mm, respectively.

A compact and portable design of a brain scanner has been introduced by Brain Biosciences, the so-called CerePET. It weighs approximately 23 kg. The device features LYSO crystals (2 mm × 2 mm × 13 mm), a bore diameter of 25 cm, and a 20 cm axial field-of-view. Preclinical work with phantoms showed a spatial resolution in the range from 2 mm to 3 mm across the field-of-view with an energy resolution of 13% [11].

A completely new design approach, in which the patient is

in the upright position, was introduced by Yamamoto, as the PET-Hat concept, at the Kobe City College of Technology (Japan) [12]. Fig. 3 (a) shows a photograph of the system. The detector block design is based on two GSO layers and a tapered light guide coupled to a flat panel photomultiplier. The tapered light guide is used to increase the size of the GSO blocks and reduce the number of PMTs used for the PET. The scintillator pixels are 4.9 mm × 5.9 mm × 7 mm for the inner layer, but 8 mm thick for the outer layer. Sixteen detector blocks are arranged in a 280 mm diameter ring defining a transaxial and axial FOV of 200 mm and 48 mm, respectively. An energy resolution of the block detectors of about 15% FWHM and a timing resolution of 4.6 ns FWHM, were respectively determined. Transaxial and axial resolutions at the centre of the FOV were reported to be 4.0 mm and 3.5 mm, respectively, together with a sensitivity of 0.7% at the centre of the axial FOV.

Following the advantages of compact brain PET designs, an NIH funded Bran Initiative grant to the AMPET collaboration (West Virginia University, UC Davis, Washington University, and General Electric GRC, Niskayuna, NY) aims at showing a motion free wearable brain PET system [13][14]. It requires sophisticated mechanics to permit relatively free and safe motion, see Fig. 3 bottom. Self-supported and robot-supported ring and helmet type imagers are envisaged. Additional challenge is that optimized high efficiency detector designs require large coverage and heavier detectors. Here, Silicon Photomultipliers (SiPMs) are used to achieve system compactness.

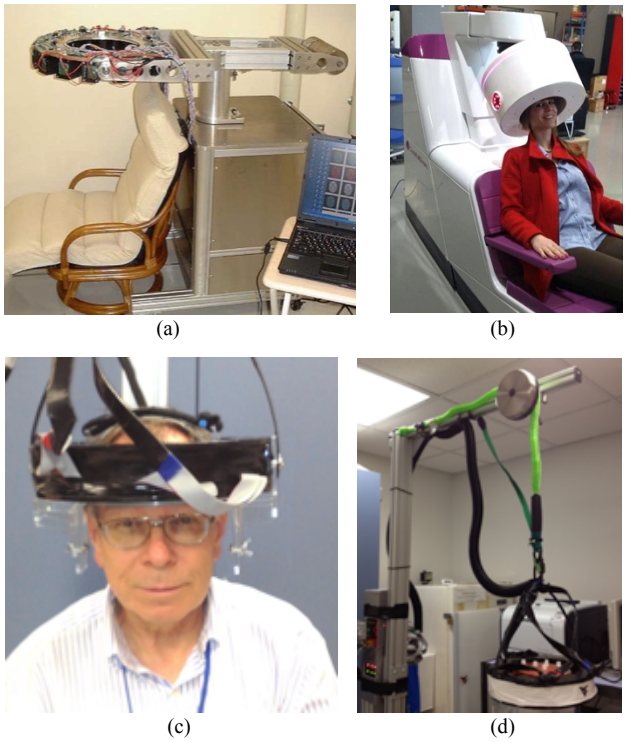

(a) (b) (c) (d)

Fig. 3. Some upright brain PET approaches. (a) PET-Hat design from [12]. (b) Upright position of the CareMiBrain (Oncovision). (c)-(d) Portable brain PET (AMPET), images courtesy of S. Majewski.

Measuring and using the photon DOI information has a strong image quality impact at the border of the image FOV [15]. This becomes more important for compact structures. The jPET-D4 PET scanner introduced a four-layer DOI scheme achieving high sensitivity and uniform spatial resolution [16]. A uniform spatial resolution of 3 mm together with a sensitivity of 11.3 ± 0.5% (at the center of the FOV, CFOV) is reported. However, about three-fourths of this sensitivity is related to multiple-crystals events. The scanner has a FOV of 25 cm in diameter [17]. This concept has been used for brain imaging following a semispherical geometry with even additional detectors located at the patient chin and, thus, the geometrical sensitivity for a region-of-interest at the center increased by 200%. Compared with standard whole-body cylindrical PET, the proposed geometries can achieve 2.6 times higher sensitivity for brain regions [18].

Providing DOI information is considered one of the intrinsic advantages of monolithic crystals. In this sense, a stand-alone brain PET system, with the patient also in upright position, named CareMiBrain, has been recently proposed, see Fig. 3 (b). It has been designed using LYSO blocks of 50 mm × 50 mm × 15 mm. The system reaches an axial and transaxial FOV of roughly 150 mm and 240 mm, respectively. The single LYSO blocks are coupled to arrays of 12 × 12 SiPM, but only 16 signals per block are needed to accurately provide 3D photon impact position [19]. The detectors have shown uniform spatial and energy resolutions of 1.8 mm (without corrections for the source size used in the measurements, 1 mm in diameter) and 13%, respectively. Also, a DOI resolution of 3.7 mm has been reported. The whole assembly is currently under performance evaluation, and a multi-clinical research will follow.

B. Brain SPECT

Although PET provides the highest sensitivity and allow for quantitative measurements, SPECT functional brain images reach similar spatial resolutions [2]. The variety of radiopharmaceuticals available for brain SPECT is not as great as that for PET, however it is expanding rapidly. Recent developments make it possible to extract kinetics from dynamic SPECT data acquired using detectors that rotate while radiopharmaceuticals exchange between biological compartments [20].

Initial SPECT studies in dynamic brain imaging were carried out as early as 1963 [21] using two and, later, four discrete detectors [22]. In 1990, SPECT brain imaging was realized with a rotating four-headed gamma camera system [23]. Also, dedicated brain systems consisting of a ring of scintillation detectors were developed [24][25]. These included the SPRINT system [24] developed at the University of Michigan; the Cleon Brain SPECT system originally developed by the Union Carbide Corporation in the 1970s, which consisted of 12 detectors that scanned both radially and tangentially [26]; ASPECT, a dedicated brain system [27]; and the FastSPECT system [28] developed at the University of Arizona, which was reported to be able to acquire dynamic tomographic data with a sampling interval of 2 s. A system

with multiple rings of scintillation detectors was also developed for brain SPECT studies in Japan by Shimadzu. The system consisted of 64 NaI crystals in a 38 cm diameter circle [25].

Just to mention some brain SPECT systems currently in use, the Massachusetts General Hospital (MGH) in Boston has the availability for a brain dedicated SPECT [29]. Sensitivity near the center of the brain is critical for some clinical applications of brain SPECT, especially for those applications which require dynamic imaging. This dedicated brain SPECT system uses variable focusing to increase the sensitivity for central regions of its field of view without compromising spatial resolution. The scanner consists of a single ring of NaI crystal (internal diameter 31 cm, height 13 cm and thickness 8 mm) and, therefore, provides a significant higher sensitivity than systems based on multiple heads. The crystal is coupled to 63 PMT arranged in three contiguous rings [30].

C. Multimodal brain imaging systems

In brain imaging, as in most of other imaging modalities, combining functional and anatomical information becomes very important, but also technologically challenging. This complementary information helps clinicians to better localize the lesion under study. The predominant type of anatomical and functional imaging combination in brain has been PET and CT. Sequential acquisition of both modalities is currently possible, but not simultaneous since it is hard to isolate the PET electronics from the CT radiation noise. However, in the last decade there has been a significant push forward to develop simultaneous PET-MRI brain imaging. Note that whole-body PET-MRI systems have also been used for brain studies [31].

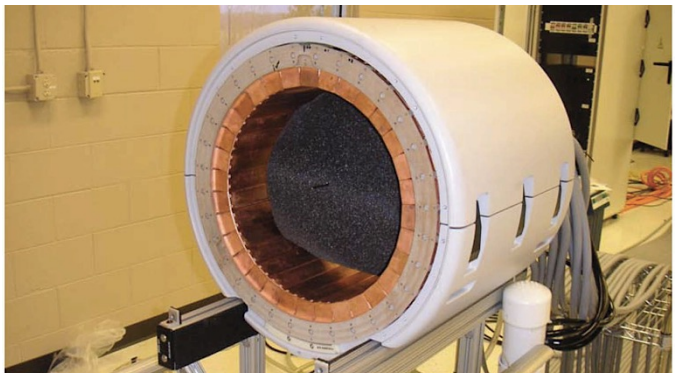

Fig. 4. Photograph of the BrainPET insert, from [34].

Commonly known as the first brain PET insert is the one developed in Jülich (Germany). The so-called BrainPET was combined with the Siemens MAGNETOM Trio MRI [32][33][34]. Six 12 × 12 arrays of 2.5 mm × 2.5 mm × 20 mm LSO crystals are read out by 9 Avalanche Photodiodes (APDs). APDs are solid-state photodetector technology, working in the avalanche regime. They are sensitive to moderate-high temperatures with proportional increase of their intrinsic dark counts. Thus, temperature controlled environments are preferred for the implementation of these systems (see Fig. 4).

Only few years later, at the department of Electronic Engineering of the Sogang University in Seoul, it was introduced the first brain PET insert based on SiPMs [35]. The system contains 72 detector blocks on a ring structure of 330 mm aperture (250 mm transaxial and 12.9 mm axial FOV), and it reaches 0.33% sensitivity. LYSO crystals of 3 mm × 3 mm × 20 mm are used. The SiPM signals are transmitted to preamplifiers using a 300 cm flexible flat cable. An average energy resolution of 18.1±2.1% is reported together with an average timing resolution of 4.2±0.2 ns. The spatial resolutions of a reconstructed point source ranges from 3.1 to 6.6 mm, at center and at 10 cm radial offset of the FOV, respectively.

A similar approach was followed at the National Institute of Radiological Sciences in Japan, also using SiPMs. A particular characteristic of this design is the use of four-layer DOI detectors integrated with the head coil of the MRI [36]. SiPMs arrays had 4 × 4 readout pixels. LGSO scintillators are arranged in 12 × 4 × 4 layers with reflectors inserted between them. The size of each crystal element was 2.9 mm × 2.9 mm × 5.0 mm. The detector and some electric components are packaged in an aluminum shielding box. A birdcage-type RF coil is used and simultaneous measurements with no influence of the MRI shown. A slight influence of the PET detector on the static magnetic field of the MRI was observed near the PET detector [37].

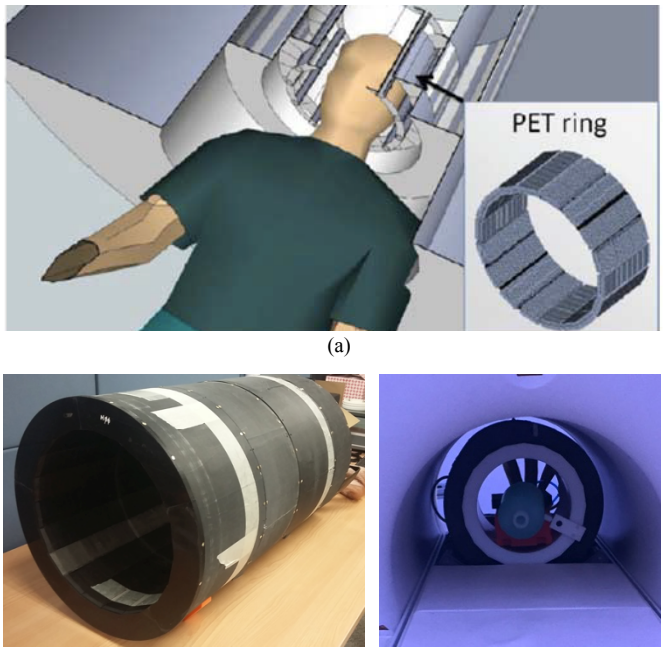

Fig. 5. (a) Sketch of the TRIMAGE approach showing the PET insert ring, RF coil and main magnet, from [39]. Bottom, MINDView photographs of the PET insert alone (b) and inside an MR installed together with the RF coil (c).

In 2013 two projects were granted at the European Union (EU) to build dedicated brain PET systems, to be MR compatible. The TRIMAGE research project develops an integrated brain PET-MRI-electroencephalogram (EEG) scanner. The MRI has a compact 1.5-T cryogen-free magnet and the PET scanner is based on SiPM technology [38]. Two

LYSO crystal arrays layers with 8 (entrance layer) and 12 mm (exit layer) height, and 3.3 mm pixel size will be mounted. The inner PET diameter is 31.2 cm and the axial length is 16.7 cm. Fig. 4 (a) shows design schematics of this system [39]. The second research project, named MINDView, is developing a PET insert intended to be an upgrade for the majority of already globally installed MRI systems [40]. It includes a radiofrequency coil that can be connected to any regular clinical MR scanner and transform the device into a high-resolution PET/MRI hybrid system, see Fig. 4 (b)-(c). The PET design is based on LYSO monolithic blocks with dimensions of 50 mm × 50 mm × 20 mm, coupled to custom SiPM arrays of 12 × 12 elements. These blocks have shown capabilities of energy resolution in the 13% range, a DOI resolution (FWHM) of 4 mm and a measured spatial resolution, on average, of 1.6 mm [41]. The transaxial and axial FOV are 240 mm (332 mm aperture) and 150 mm, respectively. It has been installed in late 2017 at the nuclear medicine department in Klinikum Rechts der Isar (Munich) and exhaustively tested inside the Siemens mMR, a whole body PET-MR with a 3T main magnetic field. A variety of MR sequences for brain imaging (including those for PET attenuation correction) have been run, and the PET response measured, not showing any performance deterioration.

Molecular brain imaging is used both in diagnostic applications and in therapy assessment. It helps providing more accurate information. Recently it has been shown the convenience of merging molecular imaging with therapy treatments, if possible simultaneously. For instance, at the MGH, clinicians have access to a mobile dedicated brain PET-CT in order to perform better planning of proton therapy, among other applications. This particular system makes use of SiPM technology for the photosensors, coupled to 2.3 mm × 2.3 mm × 10 mm LYSO crystal arrays (dual-layers). The scanner, as shown in Fig. 6 (a), is mobile and can be transported on wheels to any desired location and used with any patient bed of adjustable height [42].

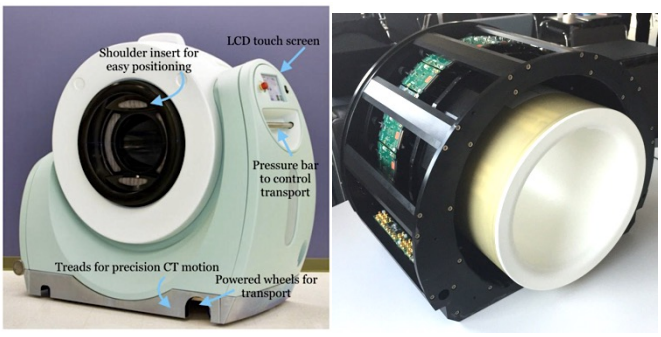

(a) (b)

Fig. 6. (a) PhotoDiagnostic system PET-CT at MGH, this figure was originally published in [42]. (b) SPECT, MR-compatible, system called INSERT, image courtesy of B. Hutton (UCL).

Hybrid SPECT-MRI systems require compact detectors that include collimation and stationary tomographic acquisitions, imposing additional constraints [43]. The main goal of the EU project named INSERT is the development of a SPECT system to be used as an insert in an MRI gantry, thus enabling the simultaneous acquisition of images resulting from the two systems. Fig. 6 (b) shows a photograph of that SPECT insert. The goal is to achieve similar performance to clinical SPECT with a compact design. A static full-ring design based on multi-pinhole has been proposed. The novelty of the design is found in the shutter mechanism that makes the system very flexible and eliminates the need for rotating parts. The target spatial resolution of this design is 6 mm [44].

IV. Breast Imaging Systems

Worldwide, breast cancer is an important healthcare issue that is responsible for significant morbidity, mortality and healthcare costs. When breast cancer is diagnosed in its earliest states it is a curable disease with a 5-year survival of greater than 90% [45]. For breast cancer diagnosis and therapy follow-up, whole-body PET devices are currently used. However, in addition to its limited spatial resolution and system sensitivity, they are bulky and expensive. Moreover, each exploration needs about 1 hour to be completed, therefore reducing the patient's throughput. Besides, radiation dose injected to the patient is in the range of 250-350 MBq (1600 mrem). Current whole-body PET is very sensitive to induced background by the radiotracer decays originated in the rest of the body, thus reducing breast exploration sensitivity.

Dedicated molecular breast imaging was made possible by developments in both fields SPECT and PET. One-side gamma cameras of a variety of photosensor types have helped radiologists and nuclear medicine physicians since many years.

A. Breast Gamma Camera

One of the systems introducing planar breast gamma imaging is the LumaGEM system (Gamma Medica Ideas Inc.) using semiconductor detectors. The camera head is composed of a pixelated (12,288 pixels) array of CZT (pixel size 1.5 mm × 1.5 mm × 5 mm) detector [46]. The camera head measures 22.5 cm × 27.7 cm × 6.6 cm. The dead space between the outside edge of the head and the active area of the field of view is less than 1 cm. The field of view is 20 cm × 15 cm. The system is modelled to have an intrinsic spatial resolution of 1.6 mm with an energy resolution of <5%, reducing scattering radiation in the image data and improving the image contrast.

Based on PSPMT and NaI(Tl) scintillation crystal arrays, the Dilon 6800 is a portable planar scintimammography gamma camera with 152 mm × 203 mm FOV [47]. It uses 3.2 mm pitch pixelated crystals. Three collimators are available: a general purpose collimator used primarily for breast imaging; a high resolution collimator used for thyroid, gall bladder, spot bone and other general nuclear medicine procedures; a Slant-15 collimator which is used for breast imaging close to the chest wall. It also allows one to carry out biopsy guidance using a specific tool.

A similar concept appeared with the Sentinella, a portable

gamma camera (1 kg weight) designed for imaging small organs and structures of the body, well suited especially for surgery scenarios [48]. The equipment is comprised of all the elements that allow for the movement of the equipment and has the necessary tools for obtaining optimum images for diagnostic and surgical purposes. The camera is based on CsI(Na) and a flat panel PSPMT. The useful field of view is 40 mm × 40 mm, with an optimal energy range of 50-200 keV (17% energy resolution at 140 keV) and an intrinsic spatial resolution of 1.8 mm.

B. Breast PET

In the field of PET imaging there have been quite many academic and commercial systems worldwide offering high performance for molecular breast imaging. High-resolution dedicated breast PET scanners have been developed over the last 10–15 years, to overcome the limitations of conventional PET scanners [49]. These systems can achieve 1.5–2.0 mm spatial resolution in the breast, thereby allowing for reliable detection of lesions in the 3–10 mm range.

The PEM Flex, compresses the breast providing 2D images similarly to those provided by an X-ray mammography. It has 2 opposing detectors mounted inside compression breast paddles [50], see Fig. 7. The detectors are 6 cm × 16.4 cm in imaging area. The detectors scan across the FOV making the maximum FOV of the system 24 cm × 16.4 cm. The detectors are constructed from 2 mm × 2 mm × 13 mm LYSO crystals coupled to PSPMT. A visualization resolution of approximately 4 mm diameter objects is possible, if they have 10 times background activity concentration, and approximately 6-7 mm objects if the activity is 4 times the background.

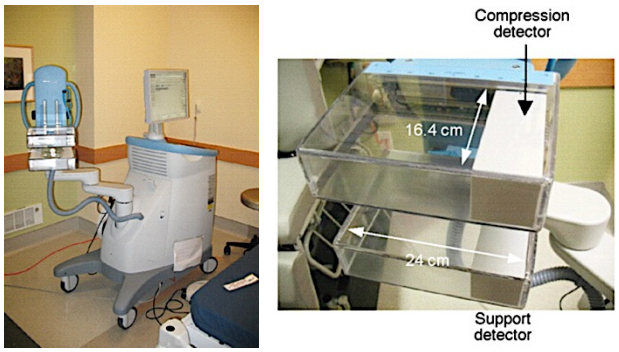

Fig. 7. Photographs and design sketch of the PEM Flex system, from [50].

With the aim of improving imaging lesions near the chest wall, it was suggested to have patients in prone position together with improved compact detector technology, as it was shown with the ClearPEM PET system [51]. This is a two panels device with adjustable distance, which can work in two modes: mild breast compression with fixed panels, or free breast with rotating panels for full tomographic reconstruction. One of the most noticeable technical advances of this system was the use of APDs, significantly reducing overall detector bulkiness, compared to the prior PMT based designs. In more detail, each panel holds 96 detector modules. LYSO crystal pixels have dimensions of 2 mm × 2 mm × 20 mm. Each side of the crystal matrix is optically coupled to a 32-pixel APD array for DOI measurements. The spatial resolution of a reconstructed small size source varies from 1.4 mm at the CFOV to 1.7 mm (transaxial) and 2.6 mm (axial) at 2.5 cm from the center. A multimodal version of the ClearPEM has also been developed including ultrasound imaging: ClearPEM-Sonic [52].

At the West Virginia University a similar two-panels approach was also implemented, see Fig. 8 (a). It used two pairs of rotating detector heads each consisting of an array of 96 × 72 pixellated LYSO crystals of 2 mm × 2 mm × 15 mm coupled to 4 × 3 arrays of PSPMT. The system FOV is 20 cm × 15 cm. It reaches about 2 mm spatial resolution in all three-dimensions, and very high event detection sensitivity (489 kcps/μCi/mL) [53].

A new work on the development of a PET system at the Stanford Medical School has been recently published, following the two panel concept combined with APD photosensor technology, see Fig. 8 (b). Initial applications were related to breast imaging, but others such as brain imaging are currently suggested [54]. Arrays of 0.9 mm × 0.9 mm × 10 mm LYSO crystal elements are used. The system reaches an active FOV of 16.5 cm × 3.3 cm. High crystal-pixel identification is reached, with an energy resolution of 11%, but exhibiting a timing resolution of almost 14 ns FWHM, most likely due to the use of APD. The 1.2 mm rods in a micro-Derenzo phantom are resolved at the CFOV (MLEM reconstruction).

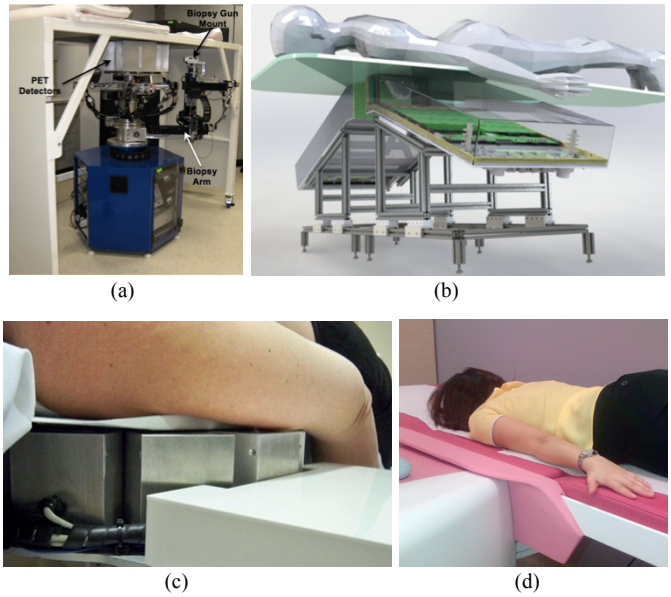

Fig. 8. (a) Photograph of the breast PET scanner developed at WVU from [53]. (b) Sketch of the organ-dedicated PET system suggested at Stanford [54]. (c) Photograph showing the MAMMI prototype ring, and (d) showing the commercial system with the patient's arm in adduction, image courtesy of Oncovision.

A breast PET system called MAMMI PET [55] (Oncovision) was developed under an FP6 EU grant called MAMmography with Molecular Imaging. The system allows

the patient to lie down in prone position with the breast freely hanging down, see photographs in Fig. 8 (c)-(d). The patient's arm on the image breast side is in adduction position helping the upper breast quadrant to be also imaged. The opposite arm is in abduction position and head tilted to the opposite breast. The PET geometry follows a ring shape with 12 (or 24 in the case of two rings) detector blocks. It makes use of monolithic 12 mm thick (50 mm × 50 mm) LYSO crystals, coupled to PSPMT, and reaches 1.8 mm spatial resolution at the CFOV [56]. The breast length in the axial dimension is covered by a step-and-shoot scan process, although the two rings approach covers about 80% of the population in one shoot.

A similar prone approach, but using crystal arrays, was used in two Shimadzu designs called O- and C-shaped, respectively [57]. The O scanner was designed for imaging patients who were in prone position, and the C scanner was designed for patients positioned inclined leaning forward, see Fig. 9 (a). Both dedicated scanners have DOI detectors consisting of a 4-layer 32 × 32 $Lu_{1.8}Gd_{0.2}SiO_5$ crystal array of 1.44 mm × 1.44 mm × 4.5 mm coupled to a 64-channel PSPMT.

With the aim to reduce system costs, an approach at the Washington University, Seattle, makes use of the concept of position sensitive sparse sensor arrays for breast (also brain) imaging systems [58], see Fig. 9. LYSO crystals of 1.93 mm × 1.93 mm × 20 mm are well resolved using only a 4 × 4 SiPM array. The PET concept follows the idea of a box shape that could allocate one or two breasts in prone position.

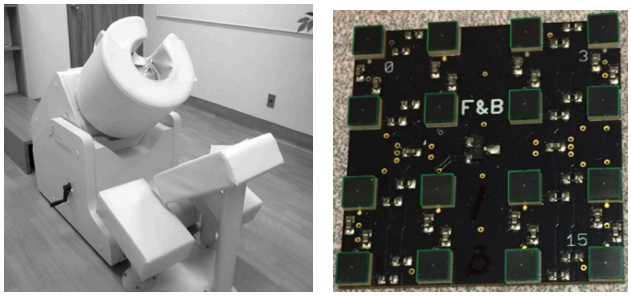

(a) (b)

Fig. 9. (a) Photograph of the C-shape PEM system, this figure was originally published in [57]. (b) Sparse detector concept.

A huge number of studies have been carried out with dedicated breast PET systems. Perhaps two of the most important applications are its high specificity as well as its capability to resolve the tumour heterogeneity. Fig. 10 shows on the top row an MR image of two breasts with predicted lesions (red-underlined). In parallel, and without crossed information, breast PET dedicated images were taken with the MAMMI system (bottom row), pinpointing just one lesion and, therefore, improving the specificity. A recent EU project (HYPMED) is developing a hybrid system of these two medical imaging modalities (MRI and PET) for improved diagnosis of breast cancer and personalised therapy control [59], see system sketch in Fig. 11 (a).

An extension of the RatCAP (rat conscious animal PET) technology from Stony Brook University has been also applied in a PET system for simultaneous breast PET-MRI imaging [60], see Fig. 11 (b). It has been successfully tested with patients. The PET ring is made out by 24 detector blocks of LYSO (4 × 8 array of crystals, where each element has a size of 2.2 mm × 2.2 mm × 5 mm) and APD arrays. The scanner has a maximum inner diameter of 100.8 mm. Using a Derenzo-like phantom, 2.4 mm rods were well resolved. However, it showed some drawbacks regarding imaging lesions that were close to the chest wall.

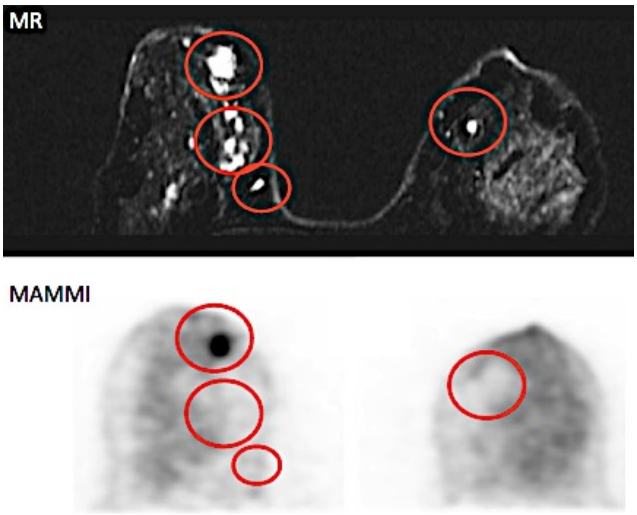

Fig. 10. Images courtesy of Dr. José Ferrer Rebolleda, Director Médico Asistencial, Ascires, Valencia, SPAIN.

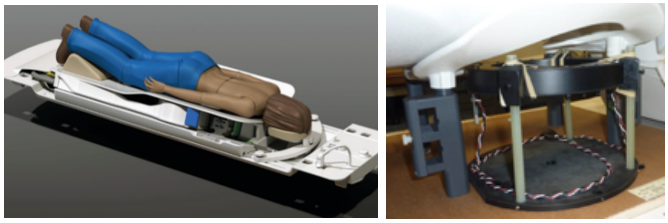

(a) (b)

Fig. 11. (a) Realization of the PET-RF coils planned in HYPMED project [59]. (b) Photograph of the implementation carried out at Stony Brook University, from [60].

C. *Breast SPECT*

SPECT systems have also been developed for breast imaging. A prototype of a combined SPECT–CT was developed and evaluated at the Pisa University [61]. The SPECT system is based on two scintillator matrices coupled to PSPMT. The heads were based on a CsI(Tl) matrix made up of 8 × 8 match-like crystals, 2.5 mm × 2.5 mm × 5 mm size. Regions of interest of 1 cm^3 were imaged with a 10:1 tumour/background concentration ratio, within an object having a diameter of 8 cm.

A compact SPECT system was designed and evaluated at the Duke University [62]. As it has been claimed for other molecular imaging systems, it served as a secondary diagnostic tool for breast cancer imaging, particularly in cases when mammographic findings were inconclusive. It was based on a gamma camera having a field-of-view of 13 cm × 13 cm with arrays of 2 mm × 2 mm × 6 mm NaI(Tl)

scintillators coupled to PSPMT. It showed an energy resolution of about 14% and an overall sensitivity of 140 cpm/μCi in a [−10%, +15%] energy window.

The Delft University and MILabs have recently suggested a new breast SPECT design concept. The breast is scanned by translating focusing multi-pinhole plates and NaI(Tl) gamma detectors together in a sequence that optimizes count yield from a volume of interest [63]. The system shows an improved contrast-to-noise ratio when compared to planar MBI by 12% for 4.0 mm lesions, increasing to 92% in a scan that focuses on a breast region containing several lesions.

V. Heart Imaging Systems

Recent decades have seen large decline trend in cardiovascular disease (CVD), and coronary artery heart disease (CAD) mortality, with rates of CVD mortality falling by >30% in both sexes and CAD mortality falling by a third in men and over a quarter in women [64]. CVD still remains the leading cause of mortality, premature death and morbidity in developed countries, causing almost 4.1 million deaths per year in the European Union alone. This figure represents 46% of all deaths in Europe. The control of CVD (and CAD) risk factors in primary prevention is generally poor and inadequately controlled [65]. Cardiac imaging has gained worldwide acceptance to detect and characterize extent and severity of cardiovascular diseases by non-invasive means.

CAD has been a particular target of new diagnostic procedures. Using quantification techniques such as molecular imaging, allows one determination of absolute parameters providing benefits in several clinical scenarios [66]. Currently, the most robust technique to quantify perfusion noninvasively in human heart is PET. Technical advances as well as preventive measures have resulted in an impressive decline of mortality based on coronary artery disease in recent years.

Since CAD becomes symptomatic during physical activity, most diagnostic procedures are linked to exercise procedures. Although flow reserve has been shown to be of incremental value for prognosis [67], it seems that absolute hyperemic myocardial blood blow outperforms myocardial flow reserve in the noninvasive diagnosis of functionally relevant CAD. These findings pave the way for stress-only protocols, obviating the need of resting perfusion imaging. However, these physical activities are today limited due to the technical requirements of imaging devices (supine position, large imaging gantry, motion artifacts…).

A. Heart PET

Very recently, some dedicated specific PET systems devoted to cardiac studies have been developed (Attrius PET, Truesight PET). They are based on large detector structures, mainly based on conventional Whole Body (WB) geometries, and are not optimized from the sensitivity and resolution point of views for the specific organ under study (human heart), see Fig. 12. These systems make use of previous generation PSPMT technology and crystal arrays. Attrius PET scanner, with a weight of 2500 kg, uses 8.5 mm × 9.8 mm × 30 mm BGO crystals arranged in 24 rings, 128 pixelated crystals each, read out by a total of 768 PMTs. With an axial FOV of 123.6 mm and a ring diameter of 78 cm, it has a spatial resolution of about 5.8 mm and a sensitivity of 200×10^3 counts/s/μCi/cc. Using BGO crystal implies a coincidence resolving time (CRT) of 6 ns, well above the values obtained for LYSO based PET systems, where CRTs of 500 ps are nowadays obtained. There is a new version of Attrius scanner (Attrius L PET) with 32 rings and an axial FOV of 166 mm, thus increasing the sensitivity up to 280×10^3 counts/s/μCi/cc, whit no significant variation on other parameters. Heart dedicated specific PET systems with modular and optimized geometry in order to attain the highest possible angular coverage of the human heart are desirable.

Fig. 12. Truesight cardiac PET system from Neusoft Medical, photograph, from http://medical.neusoft.com.

The design of an ideal heart dedicated PET should consider the actual size and position of the human heart in the body, as well as to allow patient motion during scan, especially for tests under heart stress situation, see Fig. 13. At present, there are no imaging techniques that are able to evaluate the functional operation of the heart while performing exercise and that permit limited movement of the patient. Current protocols visualize heart operation under induced stress but not under realistic upright exercise conditions. In the cardiac stress test, this heart condition is artificially induced through the use of stress drugs that are associated with considerable side effects. In a design, where a panel PET geometry would be fixed and only patient motion is allowed, 3D position markers are necessary to transmit patient-PET relative position to the data acquisition system for recording and inclusion in the reconstruction algorithm [68]. Several reconstruction algorithms could be implemented to take into account the actual patient position, obtaining the reconstructed image in a fixed-like reference frame. In this way, motion artifacts, normally present during PET scans (i.e. respiratory motion) can be truly monitored and compensated in the final image.

Considering the dimensions and position of the human heart (see also Fig. 13), optimal scanner design should be asymmetric, assuring the covered solid angle in the front and rear panels is equivalent ($\Omega1 = \Omega2$) and, therefore, maximizing the sensitivity in the heart location. For typical heart dimensions (12 cm in length, 9 cm wide, and 6 cm in thickness), sensitivity for a point-like source located at the

center of the heart position has been reported, using Monte Carlo simulation tools, to be about 16.5% (LYSO, 20 mm thick) for a front panel of 24 cm × 18 cm and a rear panel of 48 cm × 36 cm [69]. However, such atypical detector system geometry presents special challenges. It requires excellent determination of the photons TOF (to overcome the problem generated by the limited angle geometry) and DOI (to deal with the small detector panel distance that increases the parallax error).

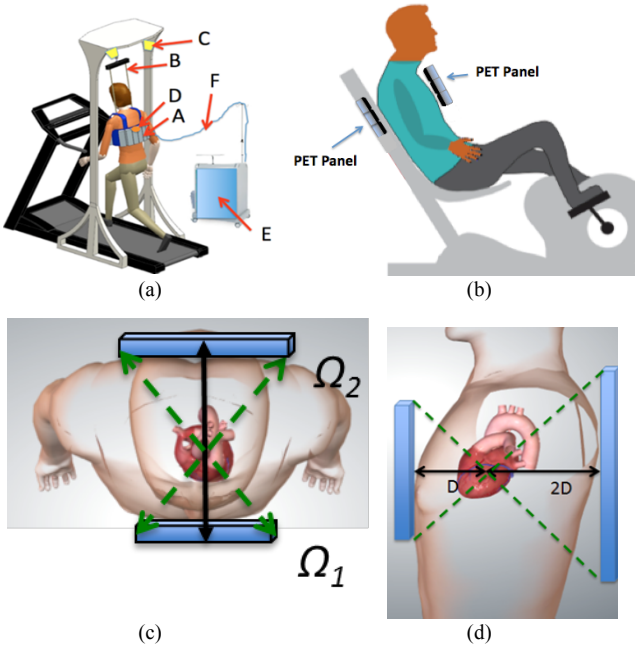

Fig. 13. (a)-(b) Dedicated heart PET scanners allowing patient movement to induce heart stress. (c)-(d) Sketches of a heart dedicated PET scanner, with limited angle coverage (dual-panel) to allow patient movement. Typical *D* value is about 9-10 cm, although PET design should allow adjustment of PET panel distance. In this way, PET detectors can be placed as close as possible to the body in order to maximize sensitivity

B. Heart SPECT

Digirad was probably the first company to develop and manufacture a dedicated cardiac SPECT scanner (Cardius 3 XPO) [70]. Although this system was originally designed to use CZT pixelated detectors, the production models make use of pixelated CsI(Tl) detectors and photodiodes. Each detector head is 21.2 cm × 15.8 cm and contains an array of 768 (6.1 mm × 6.1 mm × 5 mm) crystals coupled to individual silicon photodiodes. Data acquisition is typically accomplished in 7.5 minutes by rotating the patient chair through an arc of 202.5°. With this system, the manufacturer reports a reconstructed spatial resolution of 15.4 mm and a sensitivity of 234 cpm/μCi using the system's cardiac collimator. New versions of the system have small multiple-gamma cameras that rotate to obtain sufficient angular sampling along with an x-ray transmission system for obtaining an attenuation map for attenuation correction. Since then, several dedicated cardiac SPECT scanners have been developed such as the CardiARC (Lubbock, USA) [70] or C-SPECT (Rush University Medical Center, Chicago, USA), [71]). The C-SPECT has a stationary C-shaped gantry that surrounds the left-front side of a patient's thorax. The stationary C-shaped collimator and detectors system in the gantry provide effective and efficient detection and sampling of photon emission. The collimator system is based on the "slit-slat" design and the detector assembled from many NaI(Tl)-based modules, packed side-by-side transversely.

CardiARC was also originally designed to use arrays of CZT crystals as detectors, but the production model currently uses 3 curved NaI(Tl) crystals and an array of photomultiplier tubes with proprietary digital logic. Collimation is accomplished via a thin curved lead sheet with 6 vertical slits. During acquisition, the aperture arc rotates to acquire data from multiple projections, providing 1280 angular samples in 0.14° increments over 180º. Reconstructed spatial resolution values quoted by the manufacturer range from 3.6 mm at 82 mm from the aperture arc, to 7.8 mm at 337 mm.

Several SPECT devices based on CZT solid state detectors have been recently introduced on the market that are specifically designed for cardiac studies as the D-SPECT [68][72] (Spectrum Dynamics) shown in Fig. 14, or NM 530c and NM/CT 570c [73] (General Electric). In the D-SPECT system, the patient is imaged in a semi-reclining position with the left arm placed on top of the camera. This system consists of nine pixellated CZT detector arrays mounted in a vertical column. Each detector column is composed by an array of 16 × 64 CZT elements (2.46 mm × 2.46 mm × 5 mm), collimated by a parallel-hole tungsten collimator. Each detector column is fixed in a mechanical mounting so that data acquisition can be accomplished by rotating the columns in synchrony. Spatial resolution measurements performed according to NEMA specifications via the standard line source geometry have been reported by the manufacturer to average 4.36 mm FWHM. NM 530c from General Electric combines a multi-pinhole collimator block interfaced with a multidetector array of 2.46 mm × 2.46 mm pixelated CZT modules. The whole system detector contains 19 detector heads of 8 cm × 8 cm. Unlike traditional pinhole collimation that uses magnification, in this system minification is used. In this case the system resolution is preserved because of the small pixels and high intrinsic resolution of the CZT technology. A sensitivity of 656.8 c/s/MBq, an energy resolution of 5.4% at 140 keV and a central, tangential and radial spatial resolutions of 6.1, 3.1 and 4.3 mm, respectively, have been reported.

However, despite recent efforts to obtain PET-like quantitative accuracy results from SPECT images [74][75][76], PET still has the unique ability to measure absolute radiotracer concentrations with much higher sensitivity than any other conventional nuclear imaging technique [77], allowing the estimation of cardiac metabolism from dynamic images after bolus injection of either ^{15}O-water, ^{13}N-ammonia, ^{11}C-acetate, or ^{82}Rb. However, the main disadvantage of PET cardiac tracers is the short half-life of the radioisotopes, requiring an onsite cyclotron or a ^{82}Rb generator for tracer production. This can be considered as the current bottleneck which slows the increase of the cardiac PET

technology.

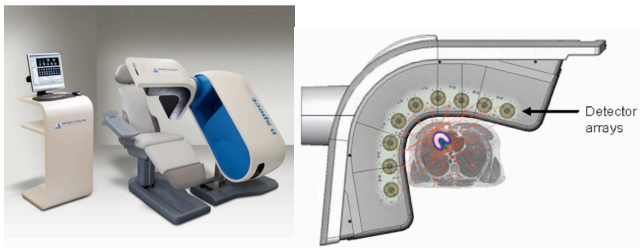

(a) (b)

Fig. 14. (a) Dedicated cardiac SPECT camera. (b) Sketch of the camera. (images from Ref. [78] © Institute of Physics and Engineering in Medicine. Reproduced by permission of IOP Publishing. All rights reserved).

VI. Other Dedicated Systems

The two panels approach, as described above for imaging the human heart or the breast, can be applied to some other scenarios. Unless large panels are used or the panel-to-panel distance is short enough to minimize the limited angle geometry, good quality TOF information of the annihilated photons is a must to return accurate and quantitative images.

In Europe, Prostate Cancer (PCa) is the most common form of cancer in men, with an incidence rate of 214 cases per 1000 men, closely followed by lung and colorectal cancer [79]. Furthermore, PCa is currently the second most common cause of cancer death in men [80]. In addition, since 1985, there has been a slight increase in most countries in the number of deaths from PCa, even in countries or regions where PCa is not common [81]. The most commonly used method for imaging the prostate is Trans Rectal Ultrasounds (TRUS). However, less than 60% of tumours – usually advanced tumours – are visible with TRUS [82]. CT and MRI are not reliable enough in the assessment of local tumour invasion [83]. Nevertheless, MRI has here several limitations that hamper its widespread application in PCa staging: difficulties in interpreting signal changes related to post-biopsy haemorrhage and inflammatory changes of the prostate, and the significant variability amongst radiologists. PET with FDG has no role in early diagnosis of PCa because of low and heterogeneous utilization of glucose by PCa, and it has a limited role in late stage cancers [84].

One of the EU projects, but not only one, which has boosted the exploration of accurate TOF for a similar geometry is the ENDOTOFPET-US project. It aimed reaching 200 ps timing resolution, corresponding to a spatial resolution of 3 cm along the LOR in such dual-head system. A sketch is shown in Fig. 15 (a) [85]. The main clinical objective is to address image-guided diagnosis and minimally invasive surgery with a miniaturized bimodal endoscopic probe with a millimeter spatial resolution [86]. The clinical cases targeted by this project are prostate and pancreas tumors. Both organs are commonly examined using endoscopic ultrasound procedures through natural orifices and could benefit of the molecular information from PET images. The external plate is a detector of 23 cm × 23 cm composed of 256 elements of 4 × 4 array of 3 mm × 3 mm × 15 mm LYSO crystals individually coupled to a matrix of SiPM [87]. An internal probe was designed and composed of a commercial transrectal ultrasound probe. The probe hosts a matrix of 18 × 18 LYSO crystals of 0.71 mm × 0.71 mm × 10 mm, coupled to digital silicon photomultiplier (dSiPM). A coincidence time resolution of 212 ± 22 ps has been reported.

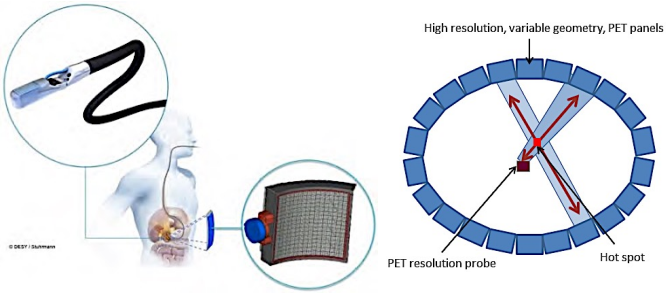

(a) (b)

Fig. 15. (a) Drawing corresponding to the endoscopic PET probe and external panel, as suggested by the ENDOTOFPET-US project. (b) Representation of the magnification effect, using a PET probe near the imaging object/organ surrounded by an external PET.

Implementation of a small probe with very high performance placed near the organ under study, allows one to improve the overall system performance, see Fig. 15 (b). Efforts in this direction to study PCa have been carried out in a collaboration between the University of Michigan and West Virginia University [88]. The improvement comes from the natural PET geometrical magnification effect, and a schematic is shown in Fig. 15 (b). In a similar approach, the so-called tandem PET method also shows to be a good solution when a high resolution probe is used. The tandem detector system consists of one detector with small detector elements (high-resolution) and another, bigger in size, with larger area detector elements (lower-resolution). This solution can potentially be used to create a system with high spatial resolution in the plane parallel to the detector without significantly increasing expense, since the total amount of scintillator and electronics is relatively small compared to most of the currently high-resolution ring scanners [89].

Some design attempts have been carried out combining US, MRI and PET imaging capabilities, in one compact probe [90]. The PET probe is suggested to include small size crystal arrays, coupled to SiPM, an MR compatible photosensor. Another approach for PET prostate imaging, but intending to avoid the use of a probe, by using two panels with an asymmetric design is currently under study at the Institute for Instrumentation in Molecular Imaging (i3M, Valencia, Spain), see details in Fig. 16. The proposed geometry, as well as it was described for the heart case, maximizes system sensitivity at the prostate location, located at about 2/3 from the abdomen-anus distance. Detector electronics with TOF capabilities will reduce the image deformation. The design is based on monolithic LYSO crystals (50 mm × 50 mm × 15 mm) with DOI information [19][91].

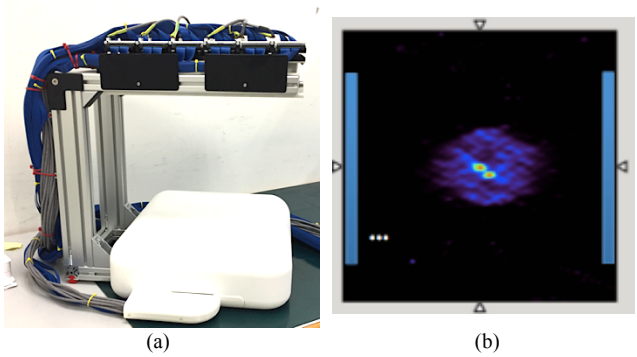

(a) (b)

Fig. 16. (a) Photograph of a dedicated two-panels PET for prostate cancer detection. (b) Simulated prostate and two lesion-sources (1 mm diameter size). The blue bars illustrate the detector panels, not in the exact position.

VII. Future Developments, Future Imaging

High specificity molecular imaging agents are suggested to drive molecules for theranostics. If the molecules bind fundamentally to prostate cancer cells (other tumor cases would be specifically applicable), they could be used to drive the chemotherapy to PCa specific cells, therefore minimizing the secondary effects. Thus, there is an indication of combining dedicated molecular imaging systems with the development of theranostic drugs based on Prostate Specific Monoclonal Antibodies (PSMSA) targeting molecular imaging agents.

The application of nanotechnology to medicine is building a new scenario for the development of the pharmaceutical and biotechnological industry in the coming years [92]. In the particular case of cancer chemotherapy, the administration of therapeutic molecules and genes has evolved in the last decade to the application of synthetic nanodevices as vehicles for the intracellular diffusion of drugs [93]. The ultimate objective is to develop a system stable in biological fluids, in order to carry a significant amount of the therapeutic agent to cancer cells with no premature release, and introducing a controlled release of the drug through selective interaction with some intracellular components [94]. In this new scenario, organ-dedicated MI devices with increased sensitivity and spatial resolution play a crucial role in therapy follow-up and theranostics applications.

The authors can think of many other scenarios where dedicated MI systems will soon play an important role. Most of the systems described along this review are currently used either for diagnostic purposes or, in some cases, for treatment assessment. However, it is unlikely that they are used for screening or during surgery. One of the drawbacks of those two applications, especially when talking about PET, is the fact that a radiotracer is needed. That constrains its use for screening purposes. Positron emitter radiotracers suitable for accurate imaging (low positron energies) are typically only obtained in cyclotrons and have short lifetimes, what makes them difficult to use if the tests are carried out far from the cyclotron place. Improving techniques using high energy positron emitters, combined with high performance dedicated systems, are necessary.

Radiation dose to the patient and to the medical team also limits a broader use of MI, as for instance during surgery, see sketch example of brain surgery guided using PET imaging in Fig. 17 (a). Of course, this limitation is also noticeable if dedicated systems are not efficient. Therefore, improving the physical system sensitivity of the system should be intensively investigated in the design of organ-dedicated systems, making it possible to reduce administrated doses and, therefore, patient and clinicians' exposures.

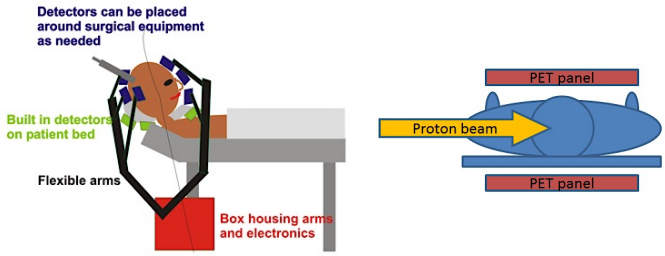

(a) (b)

Fig. 17. (a) Sketch of a brain PET for surgery with multiple modules placed flexibly around the head. (b) Sketch of a two-panels PET during proton therapy.

During surgery, one could imagine placing a PET detector panel under the patient back and a second panel (a camera) with certain motion freedom, but controlled, on top of the patient and with the organ under study in between the PET detectors. By moving the free panel and precisely knowing its space potion (optical tracking, infrared tracking, etc…), it could be possible to reconstruct, at least a part of the FOV in between the two detectors. There are currently PET image reconstruction methods capable of doing this.

Other designs for PET systems, mainly devoted for surgery applications, try to facilitate the surgeon access to the patient. A two panel PET system with a window aperture for tumor surgery guidance has been recently proposed [95]. However, sensitivity at the center is reduced by a factor of 3 if the open window in the center of the panel reaches the 44% of the panel area (see sketch in Fig. 18 left). Notice that this design implies even less angular coverage that those proposed in Fig. 13 or Fig. 16. A single-ring OpenPET enabling PET imaging during radiotherapy has also been proposed [96]. The proposed geometry has a cylinder shape cut at a slant angle, in which the shape of each cut end becomes an ellipse, as shown in Fig. 18 (b) [97]. In this case, the single-ring OpenPET shows a sensitivity 1.2 times higher than the dual-ring OpenPET proposed previously by the same authors [98]. Moreover, applications such as dose verification by in-beam PET measurement during particle therapy and real-time tumor tracking by PET require sensitivity focused onto the gap produced by the dual-ring OpenPET geometry, just the region where this geometry is less efficient.

Two additional application fields where dedicated molecular imaging devices can play an important role are: in combination with therapy treatment or biopsy guidance assistance. Molecular imaging techniques would be best suitable for determining the dose delivered to the target and to

surrounding tissues as for instance in proton (hadron) therapy, Fig. 17 (b) shows a schematic example. To effectively integrate a PET into a hadron therapy treatment centre, the system falls into the limited angle tomography types scanner. This geometry allows the beam to pass through the patient without hitting the detectors of the PET scanner. Biopsy guiding is typically complex to carry out using molecular imaging as for instance in breast or prostate cancer procedures. However, a dedicated system would allow one to safely and accurately perform these tasks. It would allow real-time visualization and 3D image reconstruction of tumours, monitoring the path of the needle inside the patient [99].

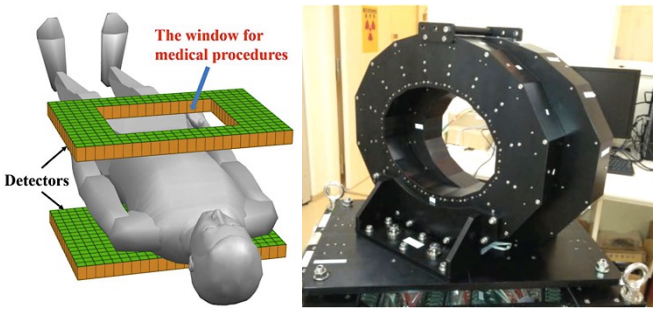

(a) (b)

Fig. 18. (a) Sketch of the PET panel window approach for surgery, from [95]. (b) Sketch of the slant approach of the OpenPET scanner [97].

Back to the idea of using two panels PET system, such a configuration could be extended to almost any organ, if accurate TOF information and photon DOI are available. The panels could, as described above, make use of optical markers to monitor their space position while acquiring data. What facilitates this approach is that these days the photodetectors are mostly done using compact solid state SiPM technology, making the PET system less bulky and, furthermore, MR compatible.

The aforementioned tandem idea could also be combined with the existing and installed whole-body PET scanner base or even with the newest total-body PET [100]. High precision detectors could be placed near the organ under study, and use the body PET as the second/coincidence detector. This image magnification idea was introduced before [101].

A scenario that we would also like to introduce in this review, and especially towards the future trends in molecular imaging, is the use of these medical techniques in rehabilitation care. Particular interest has been put in the research of innovative neuro-rehabilitation techniques, adapted through portable neuroimaging systems. One of the aims is developing portable PET technology, following some of the ideas introduced at West Virginia University [14], and combine them with Virtual Reality (VR) or/and Augmented Reality (AR) in the rehabilitation of stroke or Traumatic Brain Injury (TBI), to name but a few. VR is for instance currently under use in Alzheimer Disease rehabilitation, see Fig. 19. A very low weight PET is needed, thus compromising physical sensitivity of the system. An alternative approach is to use novel mechanical systems that hold the PET scanner or help compensating its weight, such as an exoskeleton. In collaboration with the University of Virginia, the authors have proposed a complete cylinder of BGO material (see Fig. 19 left), perhaps covered on the top with an additional block to further increase sensitivity [102]. BGO is especially interesting for this purpose because of its short attenuation length (1.1 cm for 511 keV gamma rays). BGO crystals are rather easy to grow, especially when compared to Lutetium-based fast scintillators (LYSO, LSO). Indeed, the authors have recently shown good performance of monolithic BGO blocks [103]. Although it has been shown the feasibility of reaching high timing resolution capabilities using BGO [104], it is widely known that Lutetium-based scintillators or other crystals such as LaBr3 or GAGG can provide much better timing performances. Using these types of materials will definitely improve the TOF resolution and, therefore, increase the clinical sensitivity through an improved SNR in the image. Thus, smaller volume of scintillation material could be used, making it lighter, but with similar overall systemic imaging performance.

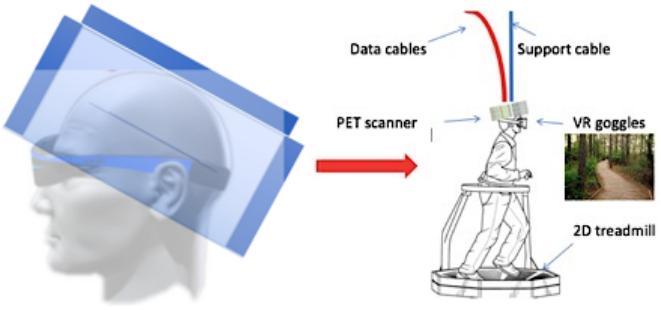

(a) (b)

Fig. 19. (a) Sketch of a brain PET made out of a full scintillation cylinder, VR goggles combined. (b) Sketch of a VR platform and a molecular imaging device. Sketch provided by S. Majewski (UVa).

VIII. Discussion

We have reviewed the varied developed molecular imaging systems for organ-dedicated applications. Some of the advantages of the organ-dedicated MI systems are their improved performance when compared to non-dedicated standard MI systems (standard whole body scanners) such as image quality and sensitivity both clinical and physical, and also their reduced cost. Other advantages arise from small footprint and higher patient throughput. Disadvantages of organ-dedicated MI techniques are mainly focusing on the examination of typically a single organ, reducing their usage by different areas or departments in a clinical center. Organ-dedicated MI systems must accomplish the "point of care". They should, at least, be portable, low cost, provide quantitative imaging, and timely feedback. Moreover, when dealing with dedicated PET scanners, the drawbacks are typically related to their geometry or detectors configuration. On one hand, small ring diameters increase the parallax error, leading to a degradation of resolution uniformity [105]. However, the simultaneous realization of small ring diameters and thus high geometric efficiency, together with high spatial resolution uniformity can be accomplished with precise

photon DOI. On the other hand, if partial detector rings are used, as for instance two panels geometry, an image quality deterioration is expected. Here, the lack of projected angular information without a precise determination of the two photons time of flight, infers a deformation of the reconstructed PET image. Current PET instrumentation trends have shown to palliate this effect by providing PET systems with accurate photons detection TOF [106].

There have been organ-dedicated system developments based on different detector block of different designs using different types of scintillators and photosensors, following evolution of the imaging instrumentation accordingly to their introduction to the market [95]. As an example, all initial designs of detector blocks started with PMTs, then moved to APDs, and now the most common type of photosensor is SiPM [107]. We envisage that digital SiPM is potentially the most logical evolution way of this technology, but other variants may also appear in the field.

Organ-dedicated molecular imaging systems will definitely take advantage of improving timing capabilities in the detector blocks design. For any of the applications mentioned above not only organ specific, but also assisting in the dedicated tasks to be carried out (diagnostic, biopsy, surgery, radiosurgery, etc…), providing this additional information, will help to improve the image SNR. The benefits are related to lowering the dose to the patient (and the clinician) or to improve the image quality. As described in the last sections, it seems that the multi-panel configuration, starting from two, will play a major role in the future of MI dedicated systems.

Multimodality is another aspect that initial organ-dedicated systems lacked. Currently this is not longer the case, and most of the developments in this field tend to include multiple imaging modalities.

ACKNOWLEDGMENTS

The authors would like to thank other members of their group at i3M for having contributed in the described projects through their multiple efforts. We would like to also thank the R&D team at Oncovision and Bruker, as well as the ProsPET consortium, for providing their support. We would like to acknowledge S. Majewski for his continuous contribution with ideas, and for reviewing the manuscript. Other colleagues in the field have also contributed and are thanked for.

This project has received funding from the European Research Council (ERC) under the European Union's Horizon 2020 research and innovation program (grant agreement No 695536). It has also been supported by the EU Grant 603002 under the FP7 program, and by the Spanish Ministerio de Economía, Industria y Competitividad under Grant TEC2016-79884-C2-1-R and through PROSPET (DTS15/00152) funded by the Ministerio de Economia y Competitividad.

REFERENCES

[1] M. Phelps, "Positron emission tomography provides molecular imaging of biological processes," Proc, Natl, Acad, Sci, 97(16), 9226–9233, 2000.

[2] M.M. Khalil, J.L. Tremoleda, T.B. Bayomy, and W. Gsell, "Molecular SPECT Imaging: An Overview," International Journal of Molecular Imaging, vol. 2011, 2011.

[3] C. Nappi and G. El Fakhri, "State of the Art in Cardiac Hybrid Technology: PET/MR," Curr. Cardiovasc. Imaging Rep. 6, 338–345, 2013.

[4] H.O. Anger, "Scintillation Camera with Multichannel Collimators," J. Nucl. Med., 5, 515-531, 1964.

[5] M.M. Ter-Pogossian, M. E. Phelps, E. J. Hoffman, and N. A. Mullani, "A Positron Emission Transaxial Tomograph for Nuclear Imaging (PETT)," Radiology 114, 89–98, (1975).

[6] M.E. Phelps, E. J. Hoffman, N. A. Mullani, and M. M. Ter-Pogossian, "Application of annihilation coincidence detection to transaxial reconstruction tomography," J. Nucl. Med. 16, 210–224,1975.

[7] A.T. Abraham and J. Feng, "Evolution of brain imaging instrumentation," Seminars in Nuclear Medicine 41, 202-219, 2011.

[8] H. de Jong, et al., "Performance evaluation of the ECAT HRRT: an LSO-LYSO double layer high resolution, high sensitivity scanner," Phys. Med. Biol. 52, 1505, 2007.

[9] L. Eriksson, et al., "The ECAT HRRT: NEMA NEC Evaluation of the HRRT System, the New High-Resolution Research Tomograph," IEEE Trans. Nucl. Scie. 49, 2085, 2002.

[10] Z. Wang, et al., "A dedicated PET system for human brain and head/neck imaging," IEEE Nuclear Science Symposium and Medical Imaging Conference (NSS/MIC), 2013.

[11] D. Beylin, et al., "High Resolution PET Scanner Optimized for Neurological Imaging," Abstract Archive RSNA, 2013.

[12] S. Yamamoto, et al., "Development of a Brain PET System, PET-Hat: A Wearable PET System for Brain Research," IEEE Trans. Nucl. Scie. 58, 668, 2011.

[13] S. Melroy, et al., "Development and Design of Next-Generation Head-Mounted Ambulatory Microdose Positron-Emission Tomography (AM-PET) System," Sensors 17, 1164, 2017.

[14] C.E. Bauer, et al., "Concept of an upright wearable positron emission tomography imager in humans," Brain Behav. 6, e00530, 2016.

[15] A.J. Gonzalez, et al., "A PET Design Based on SiPM and Monolithic LYSO Crystals: Performance Evaluation," IEEE Trans. Nucl. Scie. 63, 2471, 2016.

[16] T. Hasegawa, et al., "Evaluation of static physics performance of the jPET-D4 by Monte Carlo simulations," Phys. Med. Biol. 52, 213, 2007.

[17] T. Yamaya, et al., "First Human Brain Imaging by the jPET-D4 Prototype With a Pre-Computed System Matrix," IEEE Trans. Nucl. Scie. 55, 2482, 2008.

[18] H. Tashima, et al., "Proposed helmet PET geometries with add-on detectors for high sensitivity brain imaging," Phys. Med. Biol. 61, 7205, 2016.

[19] A. Gonzalez-Montoro, et al., Nucl. Instrum. Meth. A., in press, https://doi.org/10.1016/j.nima.2017.10.098, 2017

[20] G.T. Gullberg, et al., "Dynamic single photon emission computed tomography—basic principles and cardiac applications," Phys. Med. Biol. 55, R111, 2010.

[21] D.E. Kuhl and R.Q. Edwards, "Image separation radioisotope scanning," Radiology 80 653, 1963.

[22] E.M. Stokely, et al., "A single photon dynamic computer assisted tomograph (DCAT) for imaging brain function in multiple cross sections." J. Comput. Assist. Tomog.. 4, 230–40, 1980.

[23] K. Kimura, et al., "A new apparatus for brain imaging: four-head rotating gamma camera single-photon emission computed tomograph," J. Nucl. Med., 31, 603–9, 1990.

[24] W.L. Rogers, et al., "SPRINT: a stationary detector single photon ring tomograph for brain imaging," IEEE Trans. Med. Imaging, MI-1, 63–8, 1982.

[25] K. Ogasawara, et al., "Hypofixation and hyperfixation of 99mTc-hexamethyl propyleneamine oxime in subacute cerebral infarction," J. Nucl. Med., 41, 795–9, 2000.

[26] H.F. Stoddart and H.A. Stoddart, "A new development in single gamma transaxial tomography Union Carbide focused collimator scanner," IEEE Trans Nucl Sci., NS-26, 2710, 1979.

[27] S. Genna and A.P. Smith, "The development of ASPECT, an annular single crystal bain camera for high efficency SPECT," IEEE Trans. Nucl. Sci. 35, 654–8, 1988.

[28] J.N. Aarsvold, et al., "Modular scintillation cameras: a progress report," Proc SPIE. 914, 319–25, 1988.

[29] G. El Fakhri, et al., "Performance of a Novel Collimator for High-Sensitivity Brain SPECT," Med. Phys. 33, 209-215, 2006.

[30] F. Zito, et al., "CERASPECT: a brain-dedicated SPECT system. Performance evaluation and comparison with the rotating gamma camera," Phys. Med. Biol. 38, 1433, 1993.

[31] G. Delso, et al., "Performance Measurements of the Siemens mMR Integrated Whole-Body PET/MR Scanner," J. Nucl. Med. 52, 1914, 2011.

[32] H. Herzog, et al., "High resolution BrainPET combined with simultaneous MRI," Nuklearmedizin 2011

[33] N.J. Shah, et al., "Advances in multimodal neuroimaging: Hybrid MR–PET and MR–PET–EEG at 3 T and 9.4 T," Journal of Magnetic Resonance 229, 101, 2013.

[34] L. Caldeira, et al., "Reconstruction of PET Data Acquired with the BrainPET using STIR," IEEE Nuclear Science Symposium and Medical Imaging Conference (NSS/MIC), 2012.

[35] K.J. Hong, et al., "A prototype MR insertable brain PET using tileable GAPD arrays," Med. Phys. 40, 042503, 2013.

[36] F. Nishikido, et al., "Feasibility of a brain-dedicated PET-MRI system using four-layer DOI detectors integrated with an RF head coil," Nucl. Instr. Methods A 756, 6, 2014.

[37] F. Nishikido, et al., "Development of 1.45-mm resolution four-layer DOI–PET detector for simultaneous measurement in 3T MRI," Radiol. Phys. Technol. 8, 111, 2015.

[38] A. Del Guerra, et al., "TRIMAGE: A dedicated trimodality (PET/MR/EEG) imaging tool for schizophrenia," European Psychiatry (2018), https://doi.org/10.1016/j.eurpsy.2017.11.007.

[39] S. Ahmad, et al., "Triroc: A Multi-Channel SiPM Read-Out ASIC for PET/PET-ToF Application," IEEE Trans. Nucl. Sci. 62, 664, 2015.

[40] J.M. Benlloch, et al., "The MINDVIEW project: First results," European Psychiatry (2018), https://doi.org/10.1016/j.eurpsy.2018.01.002

[41] A. Gonzalez Montoro, et al., "Performance Study of a Large Monolithic LYSO PET Detector With Accurate Photon DOI Using Retroreflector Layers ," IEEE Trans. Rad. Plasm. Med. Scie. 1, 229, 2017.

[42] K.S. Grogg et al., "National Electrical Manufacturers Association and Clinical Evaluation of a Novel Brain PET/CT Scanner," J. Nucl. Med. 57, 646, 2016.

[43] B. Hutton, et al., "Development of clinical simultaneous SPECT/MRI," Br. J. Radiol. 91, 20160690, 2016.

[44] K. Van Audenhaege, et al., "Design and simulation of a full-ring multi-lofthole collimator for brain SPECT," Phys. Med. Biol. 58, 6317, 2013.

[45] American Cancer Society Breast Cancer Facts and Figures. 2005. http://www.cancer.org/

[46] C.B. Hruska, et al., "Proof of concept for low-dose molecular breast imaging with a dual-head CZT gamma camera. Part I. Evaluation in phantoms," Med. Phys. 39, 3466, 2012.

[47] Private communication with Bern Welch, 2018.

[48] J. Ortega, et al., "Potential role of a new hand-held miniature gamma camera in performing minimally invasive parathyroidectomy," Eur. J. Nucl. Med. Mol. Imaging, 34, 165, 2007.

[49] I.N. Weinberg, et al., "Positron emission mammography: high-resolution biochemical breast imaging," Technol. Cancer Res. Treat. 4, 55, 2005.

[50] L. MacDonald, et al., "Clinical imaging characteristics of the positron emission mammography PEM Flex Solo II," IEEE Nuclear Science Symposium and Medical Imaging Conference (NSS/MIC), 2008.

[51] M.C. Abreu, et al., "Design and Evaluation of the Clear-PEM Scanner for Positron Emission Mammography," IEEE Trans. Nucl. Sci. 53, 71, 2006.

[52] G. Cucciati et al., "Development of ClearPEM-Sonic, a multimodal mammography system for PET and Ultrasound," J. Instrum. 9, C03008, 2014.

[53] R.R. Raylman, et al., "Positron Emission Tomography-Guided Biopsy With a Dedicated Breast Scanner: Initial Evaluation," IEEE Trans. Nucl. Scie., 56, 620, 2009.

[54] F.C. David, et al., "Design and Performance of a 1 mm3 Resolution Clinical PET System Comprising 3D Position Sensitive Scintillation Detectors," IEEE Trans. Med. Imag., DOI 10.1109/TMI.2018.2799619, 2018.

[55] L. Moliner et al., "Design and evaluation of the MAMMI dedicated breast PET," Med. Phys. 39, 5393, 2012.

[56] A. Soriano, et al., "Performance evaluation of the Dual Ring MAMMI breast PET," Nuclear Science Symposium and Medical Imaging Conference (NSS/MIC), 2013.

[57] M. Iima, et al., "Clinical Performance of 2 Dedicated PET Scanners for Breast Imaging: Initial Evaluation," J. Nucl. Med. 53, 1534–1542, 2012.

[58] R.S. Miyaoka, et al., "Performance Characteristics for a Low Cost, Dual Sided, Position Sensitive Sparse Sensor (DS-PS3) PET Detector with Depth of Interaction Positioning," IEEE Nuclear Science Symposium and Medical Imaging Conference (NSS/MIC), 2017.

[59] www.hypmed.eu

[60] B. Ravindranath et al., "Results from prototype II of the BNL simultaneous PET-MRI dedicated breast scanner," IEEE Nuclear Science Symposium and Medical Imaging Conference (NSS/MIC), 2009.

[61] A. Del Guerra, et al., "A dedicated system for breast cancer study with combined SPECT–CT modalities," Nucl. Instrum. Meth. A 497, 129–134, 2003.

[62] M.P. Tornai, et al., "A 3D gantry single photon emission tomograph with hemispherical coverage for dedicated breast imaging," Nucl. Instrum. Meth. A 497, 157, 2003.

[63] J. von Roosmalen, et al., "Molecular breast tomosynthesis with scanning focus multi-pinhole cameras," Phys. Med. Biol. 61, 5508, 2016.

[64] F. Levi et al., "Mortality from cardiovascular and cerebrovascular diseases in Europe and other areas of the world: an update", Eur. J. Cardiovasc. Prev. Rehabil. 16, 333, 2009.

[65] J.R. Banegas et al., "Achievement of treatment goals for primary prevention of cardiovascular disease in clinical practice across Europe: the EURIKA study", European Heart Journal 32, 2143–2152. doi:10.1093/eurheartj/ehr080, 2011.

[66] J. Knuuti, S. Kajander, M. Maki, H. Ukkonen, "Quantification of myocardial blood flow will reform the detection of CAD", J. Nucl. Cardiol. 16, 497P, 2009.

[67] B.A. Herzog, et al., "Longterm prognostic value of 13N-ammonia myocardial perfusion positron emission tomography added value of coronary flow reserve," J Am Coll Cardiol 54, 150, 2009.

[68] J.E. McNamara, et al., "A flexible multicamera visual-tracking system for detecting and correcting motion-induced artifacts in cardiac SPECT slices", Med. Phys. 36, 1913, 2009.

[69] H. Peng, "Design study of a cardiac-dedicated PET system", Nucl. Instr. and Meth. A 779, 39, 2015

[70] J.A. Patton, et al., "Recent technologic advances in nuclear cardiology", J. Nucl. Cardiol. 14, 501, 2007.

[71] W. Chang, et al., "C-SPECT/CT-2: design concepts and performance potential", J. Nucl. Med. 49, 124P, 2008.

[72] J. W. Askew, et al., "Early image acquisition using a solid-state cardiac camera for fast myocardial perfusion imaging", J. Nucl. Cardiol. 18, 840–6, 2011.

[73] K. Erlandsson, et al., "Performance evaluation of D-SPECT: a novel SPECT system for nuclear cardiology", Phys Med Biol. 54, 2635, 2009.

[74] Ph. Ritt, et al., "Absolute quantification in SPECT", Eur. J. Nucl. Med. Mol. Imaging 38, S69, 2011.

[75] D. L. Bailey and K.P. Willowson, "Quantitative SPECT/CT: SPECT joins PET as a quantitative imaging modality", Eur. J. Nucl. Med. Mol. Imaging 41, S17, 2014.

[76] C. Michel and M. Ricard, "Quantification in SPECT/CT: Calibration, methodology during Q.Metrix software implementation", Phys. Med. 32, 348, 2016.

[77] F.M. Bengel, T. Higuchi, M.S. Javadi, and R. Lautamäki, "Cardiac Positron Emission Tomography", Journal of the American College of Cardiology 54, 1-15, 2009.

[78] G.T. Gullberg, et al., "Dynamic single photon emission computed tomography—basic principles and cardiac applications", Phys Med Biol. 55, R111, 2010.

[79] P. Boyle and J. Ferlay, "Cancer incidence and mortality in Europe 2004", Ann Oncol 16, 481, 2005.

[80] A. Jemal, et al., "Cancer statistics, 2008", CA Cancer J Clin. 58, 71, 2008.

[81] M. Quinn and P. Babb, "Patterns and trends in prostate cancer incidence, survival, prevalence and mortality. Part I: international comparisons", BJU Int. 90, 162, 2002.

[82] J.A. Smith, et al., "Transrectal ultrasound versus digital rectal examination for the staging of carcinoma of the prostate: results of a prospective multi-institutional trial", Journal Urology 157, 902, 1997.

[83] N. Lee, et al., “Which patients with newly diagnosed prostate cancer need a computed tomography scan of the abdomen and pelvis? An analysis based on 588 patients.” Urology 54(3), 490, 1999.
[84] G. Segall, et al., “SNM practice guideline for sodium 18F-fluoride PET/CT bone scans,” J. Nucl. Med. 51, 1813, 2010.
[85] C. Zorraquino, et al., “EndoTOFPET-US DAQ, designing the Data Acquisition System of a High Resolution Endoscopic PET-US Detector,” IEEE Nuclear Science Symposium and Medical Imaging Conference (NSS/MIC), 2013.
[86] T.C. Meyer, “Endo-TOFPET-US: A multimodal ultrasonic probe featuring time of flight PET in diagnostic and therapeutic endoscopy,” Nucl. Instrum. Meth. A 718, 121, 2013.
[87] N. Aubry, et al., “EndoTOFPET-US: a novel multimodal tool for endoscopy and positron emission tomography”, Journal Instrumentation 8, C04002, 2013.
[88] N. Clinthorne, et al., “Progress in development of a high-resolution PET prostate imaging probe.” IEEE Nuclear Science Symposium and Medical Imaging Conference (NSS/MIC), 2011.
[89] A.V. Stolin, et al., “Construction and Evaluation of a Prototype High Resolution, Silicon Photomultiplier-Based, Tandem Positron Emission Tomography System,” IEEE Trans. Nucl. Scie. 60, 82, 2013.
[90] F. Garibaldi, et al., “TOPEM: A PET-TOF endorectal probe, compatible with MRI for diagnosis and followup of prostate cancer,” Nucl. Instrum. Meth. A 702, 13, 2013.
[91] E. Lamprou, et al., “PET detector block with accurate 4D capabilities,” Nucl. Instrum. Meth. A, in press, https://doi.org/10.1016/j.nima.2017.11.002, 2017.
[92] Farokhzad O.C. and Langer R., “Impact on Nanotechnology on Drug Delivery,” ACS Nano 3, 16, 2009.
[93] J.R. Heath, M.E. Davis, L. Hood, “Nanomedicine targets caner,” Sci. Am. 300, 44, 2009.
[94] Mulligan R.C., “The basic science of gene therapy,” Science 260, 926, 1993.
[95] B. Li, et al., “A Panel PET With Window: Design, Performance Evaluation, and Prototype Development,” IEEE Trans. Rad. Plasm. Med. Scie. 1, 310, 2017.
[96] H. Tashima, et al., “A single-ring OpenPET enabling PET imaging during radiotherapy,” Phys. Med. Biol. 57, 4705, 2012.
[97] E. Yoshida, et al., “Development and performance evaluation of a singlering OpenPET prototype,” IEEE Nuclear Science Symposium and Medical Imaging Conference (NSS/MIC), 2012.
[98] T. Yamaya, et al., “A proposal of an open PET geometry”, Phys. Med. Biol. 53, 757, 2008.
[99] B.J. Pichler, H.F. Wehrl and M.S. Judenhofer, “Latest Advances in Molecular Imaging Instrumentation,” J. Nucl. Med. vol. 49, 5S, 2008.
[100] J.K. Poon, et al., “Optimal whole-body PET scanner configurations for different volumes of LSO scintillator: a simulation study,” Phys. Med. Biol. 57, 4077, 2012.
[101] N. Clinthorne, et al., “A high-resolution PET demonstrator using a silicon “magnifying glass”, Physics Procedia 37, 1488, 2012.
[102] C.R. Schmidtlein, et al., “Performance modeling of a wearable brain PET (BET) camera”, Proc. of SPIE 9788, 978806-1, 2016.
[103] A. Gonzalez-Montoro, et al., “Highly improved operation of monolithic BGO-PET blocks,” J. Instrum. 12, C11027, 2017.
[104] S.I. Kown, et al., “Bismuth germanate coupled to near ultraviolet silicon photomultipliers for time-of-flight PET,” Phys. Med. Biol. 61, L38, 2016.
[105] V. Sossi et al., Neuroimaging Clinics ,17,427–440, 2007.
[106] P. Lecoq, et al., “Pushing the Limits in Time-of-Flight PET Imaging,” IEEE Trans. Rad. Plasm. Med. Sci. 1, 473, 2017.
[107] C. Levin, “Promising New Photon Detection Concepts for High-Resolution Clinical and Preclinical PET,” J. Nucl. Med. 53, 167, 2012.